Supplementary Information (SI) for Journal of Materials Chemistry B.

Morphological and compositional basis of silk fiber function in *Actias luna*

Lauren E. Eccles,[1] Bert Foquet,[2] Amanda Markee,[2,3] Rebecca K. Liwang,[4] Kari B. Basso,[5] Akito Y. Kawahara,[2] Whitney L. Stoppel[1*]

[1]Department of Chemical Engineering, University of Florida, Gainesville, FL 32611, USA
[2]McGuire Center for Lepidoptera and Biodiversity, Florida Museum of Natural History, University of Florida, Gainesville, FL 32611, USA
[3]American Museum of Natural History, New York, NY 10024, USA
[4]Department of Biology, University of Florida, Gainesville, FL 32611, USA
[5]Department of Chemistry, University of Florida, Gainesville, Fl 32603, USA

*Correspondence:
Whitney L. Stoppel, PhD
1006 Center Drive
PO Box 116005
Gainesville, FL 32611
Whitney.stoppel@ufl.edu

Author contact information:
- Lauren E. Eccles – leccles@ufl.edu
- Bert Foquet – bfoquet@ufl.edu
- Amanda Markee – amarkee@amnh.org
- Rebecca K. Liwang – rebeccaliwang@ufl.edu
- Kari B. Basso - kari.basso@chem.ufl.edu
- Akito Y. Kawahara – kawahara@flmnh.ufl.edu
- Whitney L. Stoppel – whitney.stoppel@ufl.edu

All raw data is available at this link:
https://www.dropbox.com/scl/fo/7xi7izwnqrlh9sjlnzbmz/AE2gssml52ZUfinCoS3OUwc?rlkey=d4exe5vv1ynjopzl9jin1epjt&st=33be3d04&dl=0

1. Phylogenetic trees of non-repetitive FibH termini

To compare the terminal domains across phylogenetic groups, we created an N-termini, C-termini, and concatenated N/C termini tree for FibH proteins of saturniid moths. N-termini trees were generated by protein alignment of the non-repetitive exon region prior to the first repeat motif exon (**Figure 2** main text; **Figure S2**). C-termini trees were generated by alignment of terminal protein sequences after the last polyA motif and SS doublet motif (**Figure S1A, Figure S3**). Concatenated N/C termini sequences were generated by joining N-termini and C-termini sequences end-to-end into a single sequence for each species and building a phylogenetic tree through protein alignment (**Figure S1B, Figure S4**). Concatenated N/C termini trees of FibH proteins combines information from the conserved terminal region of the FibH protein, providing a more robust and comprehensive assessment of evolutionary relationships, similar to previous studies of spidroin proteins.[1, 2] Sequences from *Actias selene*, *Rhodinia fugax*, and *Saturnia japonica* were excluded from C-termini and concatenated N/C termini trees as the reported FibH sequences are partial and did not recover the C-terminal region.

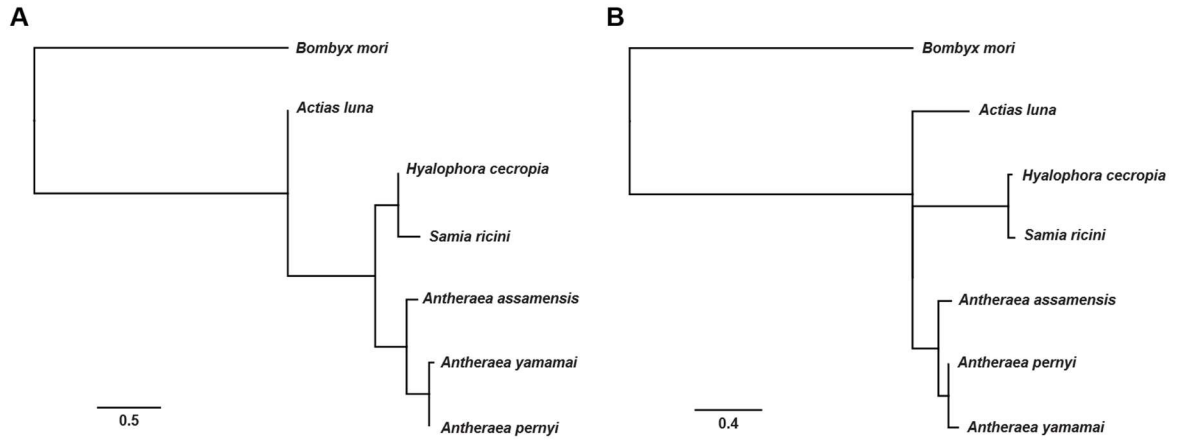

Figure S1. Phylogenetic tree generated by multiple sequence alignment of (**A**) non-repetitive C-termini and (**B**) concatenated N- and C-terminal regions of FibH proteins. Six saturniid species with complete FibH sequences were compared with *B. mori* included as the outgroup. Scale bar represents the number of amino acid substitutions per site, representative of evolutionary change. Pairwise distances between two FibH protein sequences are represented by the sum of the edges that connect them, with longer distances representing lower similarity.

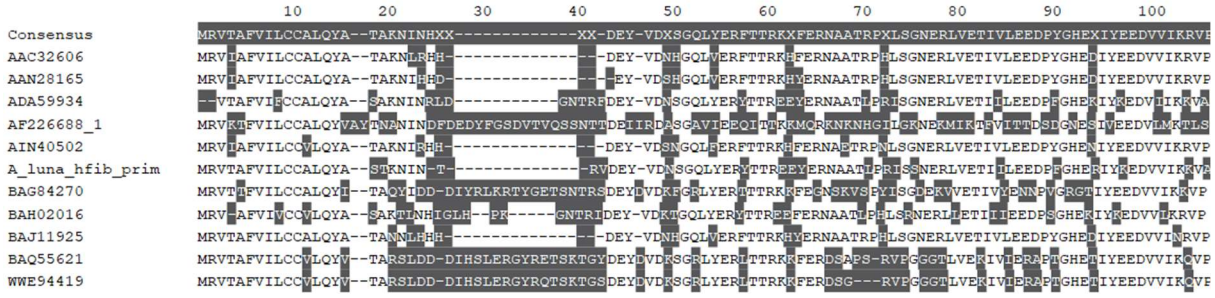

Figure S2. **Protein alignment of FibH N-terminal regions.** Alignment position numbers shown in increments of ten. Alignment prepared the multiple sequence aligner MAFFT v7.490 in Geneious Prime® v2019.2. Accession numbers and species: *A. pernyi* (AAC32606), *A. mylitta* (AAN28165), *A. selene* (ADA59934), *B. mori* (AF226688_1), *A. assamensis* (AIN40502), *A. luna* (A_luna_hfib_prim), *R. fugax* (BAG84270), *S. japonica* (BAH02016), *A. yamamai* (BAJ11925), *S. ricini* (BAQ55621), and *H. cecropia* (WWE94419).

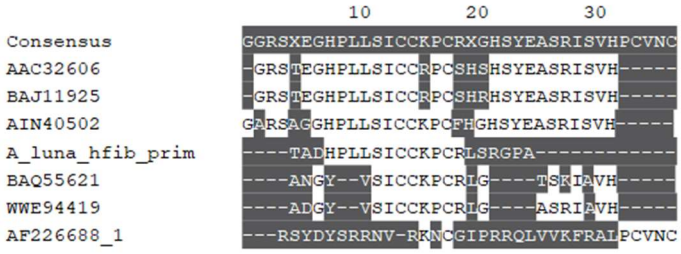

Figure S3. Protein alignment of FibH C-terminal regions. Alignment position numbers shown in increments of ten. Alignment prepared the multiple sequence aligner MAFFT v7.490 in Geneious Prime® v2019.2. Accession numbers and species: *A. pernyi* (AAC32606), *B. mori* (AF226688_1), *A. assamensis* (AIN40502), *A. luna* (A_luna_hfib_prim), *A. yamamai* (BAJ11925), *S. ricini* (BAQ55621), and *H. cecropia* (WWE94419).

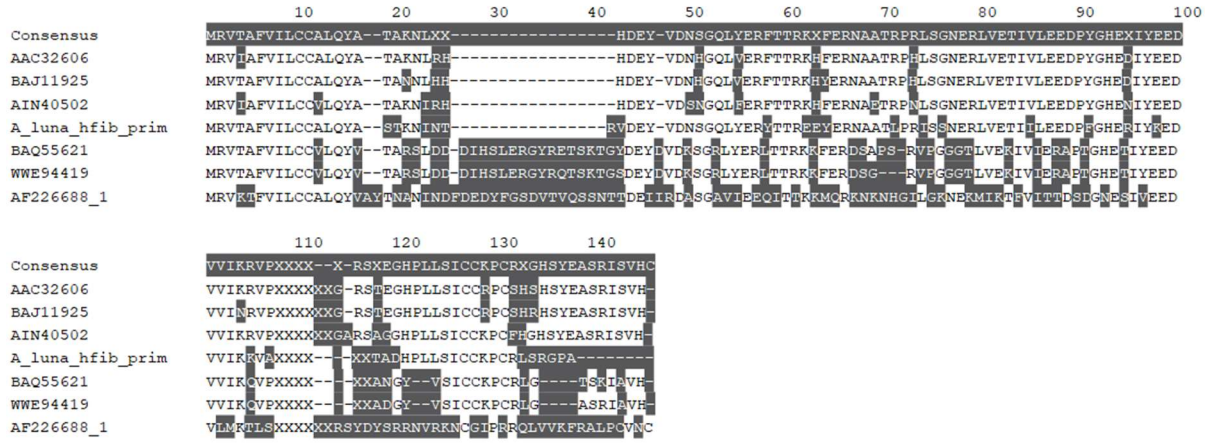

Figure S4. Protein alignment of concatenated FibH N- and C-terminal regions. Alignment position numbers shown in increments of ten. Alignment prepared the multiple sequence aligner MAFFT v7.490 in Geneious Prime® v2019.2. Accession numbers and species: *A. pernyi* (AAC32606), *B. mori* (AF226688_1), *A. assamensis* (AIN40502), *A. luna* (A_luna_hfib_prim), *A. yamamai* (BAJ11925), *S. ricini* (BAQ55621), and *H. cecropia* (WWE94419).

2. Proteomic library and assessment

Proteins were extracted and digested using the EasyPep™ MS Sample Prep Kit (Thermo Fisher Scientific). Total protein was determined on a Qubit and the appropriate volume of each sample was taken to equal 20 µg total protein for digestion. The samples were digested with sequencing grade trypsin/lys C rapid digestion kit from Promega (Madison WI) using manufacture recommended protocol. Three times the sample volume of rapid digestion buffer (provided with the kit) was added to the samples. The sample was incubated at 56ºC with 1 µl of dithiothreitol (DTT) solution (0.1 M in 100 mM ammonium bicarbonate) for 30 minutes prior to the addition of 0.54 µL of 55 mM Iodoacetamide in 100 mM ammonium bicarbonate. Iodoacetamide was incubated at room temperature in dark for 30 min. The trypsin/lys C was prepared fresh as 1 µg/µl in the rapid digestion buffer. 1 µl of enzyme was added and the samples were incubated at 70ºC for 1 hour. The digestion was stopped with addition of 0.5% TFA. The MS analysis is immediately performed to ensure high quality tryptic peptides with minimal non-specific cleavage.

Nano-liquid chromatography tandem mass spectrometry (Nano-LC/MS/MS) was performed on a Thermo Scientific Q Exactive HF Orbitrap mass spectrometer equipped with an EASY Spray nanospray source (Thermo Scientific) operated in positive ion mode. The LC system was an UltiMate™ 3000 RSLCnano system from Thermo Scientific. The mobile phase A was water containing 0.1% formic acid and the mobile phase B was acetonitrile with 0.1 % formic acid. The mobile phase A for the loading pump was water

containing 0.1 % trifluoracetic acid. 5 µL of sample is injected on to a ThermoScientific µPAC™ C18 trapping column (C18, 5 µm pillar diameter, 10 mm length, 2.5 µm inter-pillar distance) at 10 µL/ml flow rate. This was held for 3 minutes and washed with 1 %B to desalt and concentrate the peptides. The injector port was switched to inject and the peptides were eluted off of the trap onto the column. ThermoScientific 110 cm µPAC™ was used for chromatographic separations (C18, 5 µm pillar diameter, 110 cm length, 2.5 µm inter-pillar distance). The column temperature was maintained 40ºC. A flowrate of 750 nL/min was used for the first 15 minutes and then the flow was reduced to 250 nl/min. Peptides were eluted directly off the column into the Q Exactive system using a gradient of 1% B to 20%B over 100 minutes and then to 45%B in 20 minutes for a total run time of 150 minutes:

Table S1. Nano-LC/MS/MS column run times and flow rates.

Time (min)	% B	Flow Rate (nL/min)
0	1	750
3	1	750
15	5	750
15.1	5	300
100	20	300
123	45	300
130	95	300
135	95	300
135.1	1	300
150	1	300

The MS/MS was acquired according to standard conditions established in the lab. The EASY Spray source operated with a spray voltage of 1.5 KV and a capillary temperature of 200ºC. The scan sequence of the mass spectrometer was based on the original TopTen™ method; the analysis was programmed for a full scan recorded between 375 – 1575 Da at 60,000 resolution, and a MS/MS scan at resolution 15,000 to generate product ion spectra to determine amino acid sequence in consecutive instrument scans of the fifteen most abundant peaks in the spectrum. The AGC Target ion number was set at 3e6 ions for full scan and 2e5 ions for MS^2 mode. Maximum ion injection time was set at 50 ms for full scan and 55 ms for MS^2 mode. Micro scan number was set at 1 for both full scan and MS^2 scan. The HCD fragmentation energy (N)CE/stepped NCE was set to 28 and an isolation window of 4 *m/z*. Singly charged ions were excluded form MS^2. Dynamic exclusion was enabled with a repeat count of 1 within 15 seconds and to exclude isotopes. A Siloxane background peak at 445.12003 was used as the internal lock mass. HeLa protein digest standard is used to evaluate the integrity and the performance of the columns and mass spectrometer. If the number of protein ID's from the HeLa standard falls below 3200, the instrument is cleaned and new columns are installed.

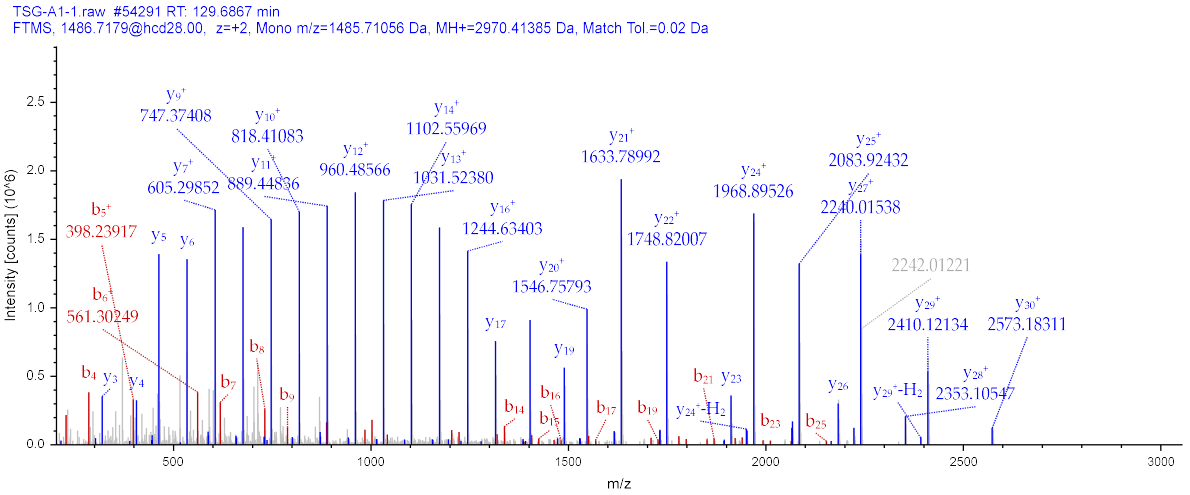

Figure S5. Example mass spectrum of a silk gland protein sample.

All MS/MS spectra were analyzed using the Chimerys node (Thermo Fisher Scientific, San Jose, CA, USA; Proteome Discoverer 3.2.0.450). Chimerys was set up to search a custom curated fasta compiled from NCBI GenBank[3] (accession numbers listed in **Table S2,** downloaded 9/15/2025)[4-9] and Universal Protein Contaminants fasta[10] assuming the digestion enzyme trypsin. Chimerys was searched with a fragment ion mass tolerance of 0.020 Da and a precursor ion tolerance of 10.0 ppm. Carbamidomethyl of cysteine was specified in Chimerys as a fixed modification. Phosphorylation of serine, threonine, and tyrosine (STY) and oxidation of methionine was specified in Chimerys as a variable modification. Precursor ion intensity label free quantitation was done using Proteome Discoverer (Thermo Fisher Scientific vs 3.2.0.450). The two groups were compared using a "non-nested" study factor. Normalization was derived by using all peptides. Protein abundances were calculated by summed abundances, meaning the protein abundances are calculated by summing sample abundances of the connected peptide groups. Precursor ion intensity label free quantitation was done using Proteome Discoverer (Thermo Fisher Scientific vs 3.2.0.450). The two groups (restricted, expanded libraries, **Table S2**) were compared using a "non-nested" study factor. Normalization was derived by using all peptides. Protein abundances were calculated by summed abundances, meaning the protein abundances are calculated by summing sample abundances of the connected peptide groups.

Table S2. Protein libraries assembled for *A. luna* silk gland proteomic analyses.

Species	Description	Accession Number/Reference	Search Library
Actias luna	Fibroin heavy chain, primary allele	[4]Markee 2024	Restricted/Expanded
Actias luna	Sericin A	XYO09379.1	Restricted/Expanded
Actias luna	Sericin B isoform 1	XYO09375.1	Restricted/Expanded
Actias luna	Sericin B isoform 2	XYO09376.1	Restricted/Expanded
Actias luna	Sericin C	XYO09378.1	Restricted/Expanded
Actias luna	Sericin D	XYO09377.1	Restricted/Expanded
Actias luna	Sericin E	XYO09374.1	Restricted/Expanded
Actias luna	Sericin F	XYO09373.1	Restricted/Expanded
Actias luna	Sericin G	XYO09372.1	Restricted/Expanded

Actias luna	Sericin 1 isoform 1	XYO09370.1	Restricted/Expanded
Actias luna	Sericin 1 isoform 2	XYO09371.1	Restricted/Expanded
Actias selene	Fibroin heavy chain	ADA59934.1	Expanded
Antheraea assamensis	Fibroin heavy chain	AIN40502.1	Expanded
Antheraea mylitta	Fibroin heavy chain	AAN28165	Expanded
Antheraea pernyi	Fibroin heavy chain	AAC32606.1	Expanded
Antheraea yamamai	Fibroin heavy chain	BAJ11925.1	Expanded
Antheraea yamamai	Src1	BBA53792.1	Expanded
Antheraea yamamai	Src2	BBA53793.1	Expanded
Antheraea yamamai	Src3	BBA53794.1	Expanded
Antheraea yamamai	Src4	BBA53795.1	Expanded
Antheraea yamamai	Src5	BBA53796.1	Expanded
Bombyx mori	All proteins from annotated genome	GCA_030269925.2	Expanded
Hyalophora cecropia	Fibroin heavy chain	WWE94419	Expanded
Hyalophora cecropia	Mucin 1-like protein	WWE94510.1	Expanded
Hyalophora cecropia	Mucin 5ac-like protein	WWE94471.1	Expanded
Hyalophora cecropia	Seroin 1 transcription variant a	WWE94430.1	Expanded
Hyalophora cecropia	Seroin 3 transcription variant a	WWE94445.1	Expanded
Hyalophora cecropia	Src1	WWE94420.1	Expanded
Samia ricini	Fibroin heavy chain	BAQ55621.1	Expanded
Samia ricini	Srp1	LC001866.1	Expanded
Saturnia japonica	Fibroin heavy chain	BAH02016	Expanded

3. Variation of degumming time on *A. luna* silk fibers

To expand on methods described by Reddy *et. al*,[11] *A. luna* silk was degummed for variable times to evaluate the overall mass loss and changes in fiber diameter. Compared to native cocoon fibers (**Figure S6A**), degummed cocoon fibers have less visual surface debris and the two fibroin filaments are separated (**Figure S6BCD**). Cocoons degummed for 15 minutes resulted in a mass loss between 18-20% and a fiber

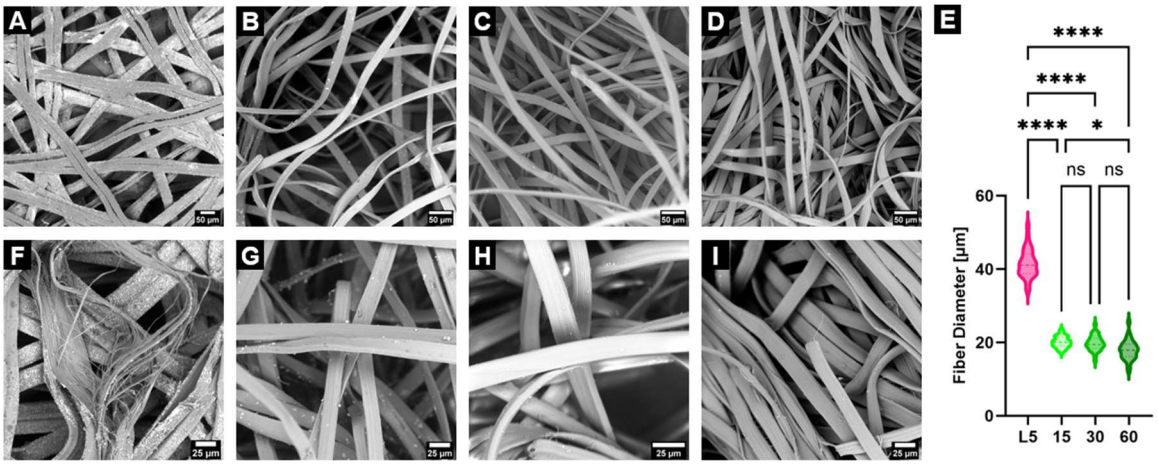

Figure S6. SEM images of degummed *A. luna* silk. Representative image of (**A**) non-degummed fibers and fibers degummed for (**B**) 15 minutes, (**C**) 30 minutes, and (**D**) 60 minutes. (**E**) Long axis fiber diameters of non-degummed and degummed fibers at each condition. Analyzed with One-Way ANOVA with Tukey's test post-hoc analysis. Statistical significance is reported as *p<0.05 and ****p<0.0001 (n=30). Higher magnification images of (**F**) non-degummed, (**G**) 15-minute, (**H**) 30-minute, and (**I**) 60-minute fibers. The internal structure of frayed or separated non-degummed fibers and external surface of degummed fibers show fibrous structures that are aligned along the axis of the fiber.

diameter of 20.1 ± 1.4 µm (**Figure S6BE**). Degumming for 30 and 60 minutes resulted in a similar mass loss, between 25-35%, and similar fiber diameters (19.4 ± 2.1 and 18.0 ± 2.7 µm, respectively) (**Figure S6CDE**). All degummed fibers exhibit a significant decrease in fiber diameter compared to native fibers ($p<0.0001$), with an average fiber diameter almost half of the native fibers, corresponding to the separation of fibroin filaments (**Figure S6E**). The difference in fiber diameter between 30 and 60 minutes was not significant, suggesting that continued removal of the outer sericin layer did not occur during longer exposure to high temperature and degumming solution. Combined with the similar mass loss observed between 30- and 60-minute degumming times, the data is sufficient to confirm that adequate removal of the outer fiber coating occurs within 30 minutes. While longer degumming times may serve to shift the

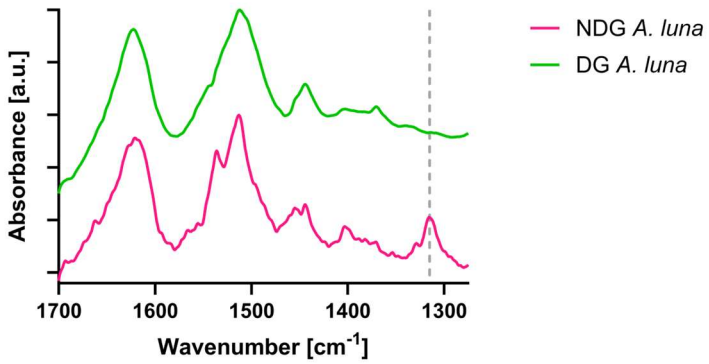

Figure S7. Representative FTIR spectra of *A. luna* non-degummed and degummed cocoon fibers between 1275-1700 cm^{-1}. The peak attributed to the presence of calcium oxalate hydrate is observed at 1315 cm^{-1}.

MW of silk fibroin through hydrolysis of the silk fibroin polymer chain, as observed in *B. mori* silk materials,[12, 13] characterization of silk fiber properties is evaluated only for 30-minute degummed silk as this is the minimum time determined for removal of the outer coating.

Degummed *A. luna* fibers have a visually smoother appearance than non-degummed fibers, with an aligned fibrous or fibrillar structure visualized at higher magnification (**Figure S6GHI**). This aligned fibrous structure is similar to the internal structure of native fibers visualized when the fibers have ripped or frayed (**Figure S6F**), suggesting that degumming processes were successful in removing the outer coating and revealing the hierarchically structured fibroin core. Calcium oxalate crystals visualized on the native silk fibers (**Figure S6F**) are gradually removed through longer degumming processes. Calcium oxalate crystals are water insoluble and largely heat resistant, often requiring longer degumming times, additional degumming agents (i.e., ethylenediamine), and high agitation to remove them from where they are embedded within or adhered to the silk fiber surface. There is a higher abundance of crystals observed on 15-minute degummed silk compared to the little to no crystals observed on the surface of 30- and 60-minute degummed silk fibers. The removal of calcium oxalate on the surface of silk fibers was also confirmed by FTIR spectra of 30-minute degummed silk, observed by the lack of a peak at 1315 cm^{-1} compared to the spectra of native fibers (**Figure S7**).

4. Sequence-function relationships within saturniid silks

The lower thermal stability and extensibility of *A. luna* silk fibers compared to other Saturniidae align with trends described in prior literature.[14, 15] To evaluate these correlations, thermal decomposition temperatures

and extensibility values are plotted as a function of FibH protein motifs correlated to rigidity (polyA, **Figure S8A**) and elasticity (GGX, **Figure S8B**) of the protein backbone, respectively. FibH protein characteristics of *A. luna* were evaluated with the primary allelic variant.[4, 15] *Actias luna* properties align with trends in saturniid silks noted in prior literature,[14, 15] wherein increasing polyA, or crystallinity, correlates to a higher thermal stability (Error! Reference source not found.**A**) and decreasing GGX motifs corresponds to lower elastic content and decreased extensibility (**Figure S8B**).

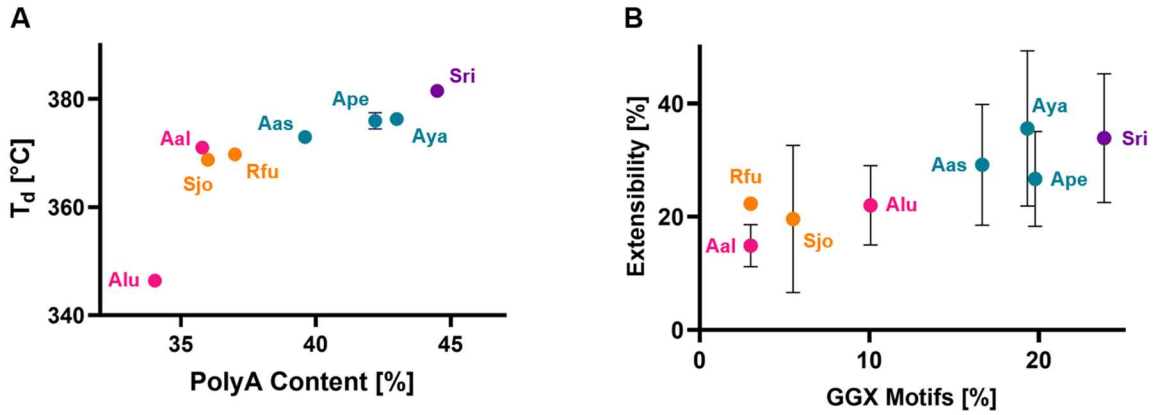

Figure S8. FibH correlations within saturniid silk fibers. (**A**) Thermal decomposition temperature versus polyA content within FibH proteins. (**B**) Extensibility versus GGX motif content within FibH proteins. Properties from other saturniid silks are reported by Malay et al.[14] Species names are colored corresponding to genus (pink: *Actias*, blue: *Antheraea*, purple: *Samia*, orange: wild).

5. Insect and fiber characteristics at each *A. luna* larval instar

To track the development of *A. luna* larva throughout their life cycle, silk fiber and larval characteristics were assessed at each life stage. Head capsule size was measured by placing larvae next to a ruler, imaging under a microscope, and then measuring the width of the head capsule in ImageJ analysis software (**Figure S9B**). Instar larval length was measured under a microscope (similar to head capsule size) as the larvae neared the end of their life stage, prior to molting (**Figure S9C**). Larval body mass was also assessed in larvae prior to molting to reduce fluctuations in mass as a function of feeding and growth during instar stage (**Figure S9D**). Silk fibers produced at each life stage were imaged by SEM and AFM for measurement of long axis fiber diameter and surface roughness (**Figure S9E**). Summary of statistical analysis for fiber characteristics are listed in **Table S3**. Analyzed with One-Way ANOVA with Tukey's test post-hoc analysis. Statistical significance is reported as ****$p<0.0001$ and ns=no significance.

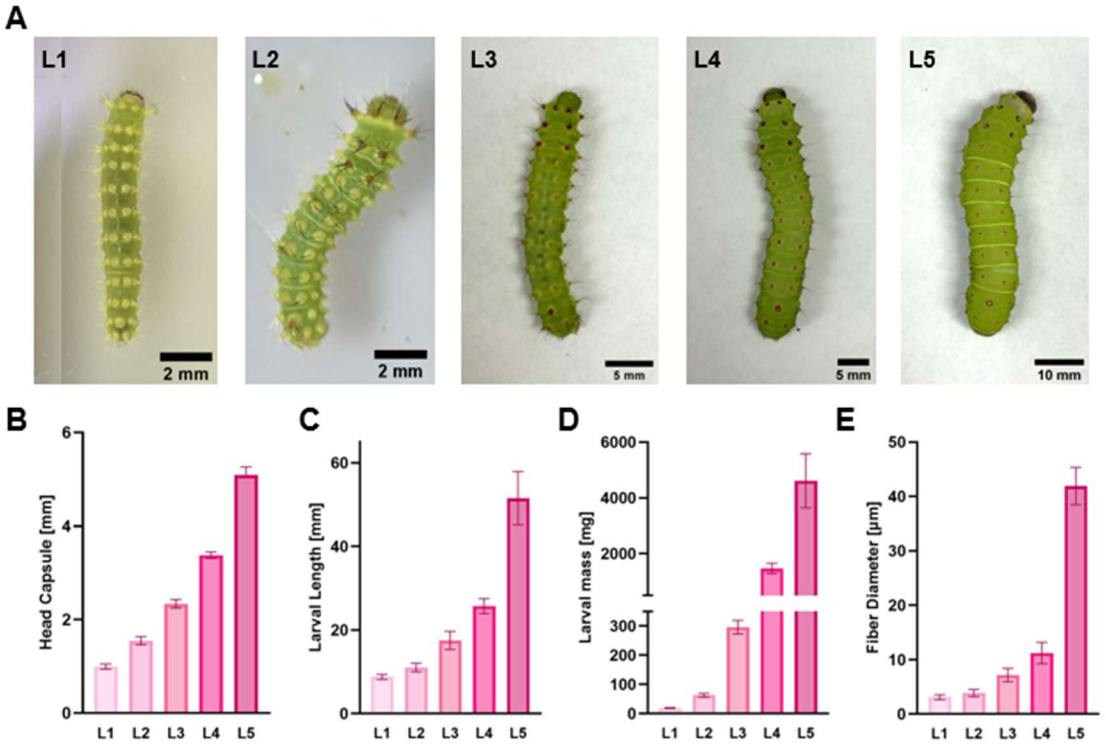

Figure S9. Trends in insect and fiber growth across life stages. (**A**) Images of *A. luna* caterpillars at each life stage. (**B**) Head capsule width, (**C**) larva length, (**D**) mass of larva prior to molting at each instar, and (**E**) average fiber diameter of silk fibers produced at each instar. Data is expressed as the mean ± standard deviation (n=10 for B-D, n=90 for E).

Table S3. Summary of statistical comparisons of instar silk fiber diameter and surface roughness.

Tukey's multiple comparisons test	Fiber Diameter		Arithmetic Roughness		Root mean square roughness	
	Summary	Adjusted P Value	Summary	Adjusted P Value	Summary	Adjusted P Value
L1 vs. L2	ns	0.0586	ns	0.9967	ns	0.9774
L1 vs. L3	****	<0.0001	ns	0.9706	ns	0.9455
L1 vs. L4	****	<0.0001	ns	0.9348	ns	0.9466
L1 vs. L5	****	<0.0001	ns	0.7776	ns	0.7289
L2 vs. L3	****	<0.0001	ns	0.9986	ns	0.9998
L2 vs. L4	****	<0.0001	ns	0.989	ns	0.9994
L2 vs. L5	****	<0.0001	ns	0.9202	ns	0.9559
L3 vs. L4	****	<0.0001	ns	0.9993	ns	>0.9999
L3 vs. L5	****	<0.0001	ns	0.98	ns	0.9831
L4 vs. L5	****	<0.0001	ns	0.9987	ns	0.9941

References

1. Baker RH, Corvelo A, Hayashi CY. Rapid molecular diversification and homogenization of clustered major ampullate silk genes in Argiope garden spiders. PLoS genetics. 2022;18(12):e1010537. Epub 20221212. doi: 10.1371/journal.pgen.1010537. PubMed PMID: 36508456; PMCID: PMC9779670.

2. Wang K, Wen R, Jia Q, Liu X, Xiao J, Meng Q. Analysis of the Full-Length Pyriform Spidroin Gene Sequence. Genes (Basel). 2019;10(6):425. Epub 20190603. doi: 10.3390/genes10060425. PubMed PMID: 31163680; PMCID: PMC6627382.

3. Sayers EW, Beck J, Bolton EE, Brister JR, Chan J, Connor R, Feldgarden M, Fine AM, Funk K, Hoffman J, Kannan S, Kelly C, Klimke W, Kim S, Lathrop S, Marchler-Bauer A, Murphy TD, O'Sullivan C, Schmieder E, Skripchenko Y, Stine A, Thibaud-Nissen F, Wang J, Ye J, Zellers E, Schneider VA, Pruitt KD. Database resources of the National Center for Biotechnology Information in 2025. Nucleic Acids Res. 2025;53(D1):D20-D9. doi: 10.1093/nar/gkae979. PubMed PMID: 39526373; PMCID: PMC11701734.

4. Markee A, Godfrey RK, Frandsen PB, Weng YM, Triant DA, Kawahara AY. De Novo Long-Read Genome Assembly and Annotation of the Luna Moth (Actias luna) Fully Resolves Repeat-Rich Silk Genes. Genome Biol Evol. 2024;16(7):evae148. doi: 10.1093/gbe/evae148. PubMed PMID: 38957923; PMCID: PMC11258402.

5. Foquet B, Eccles LE, Markee A, Triant DA, Frandsen P, Stoppel W, Kawahara A. Evolution of highly repetitive silk genes in the Luna moth, Actias luna. bioRxiv. 2025:2025.08. 07.669095.

6. Rouhova L, Podlahova S, Kmet P, Zurovec M, Sehadova H, Sauman I. A comprehensive gene expression analysis of the unique three-layered cocoon of the cecropia moth, Hyalophora cecropia. Insect Biochem Mol Biol. 2024;171:104152. Epub 20240627. doi: 10.1016/j.ibmb.2024.104152. PubMed PMID: 38944399.

7. Zurovec M, Yonemura N, Kludkiewicz B, Sehnal F, Kodrik D, Vieira LC, Kucerova L, Strnad H, Konik P, Sehadova H. Sericin Composition in the Silk of Antheraea yamamai. Biomacromolecules. 2016;17(5):1776-87. Epub 20160419. doi: 10.1021/acs.biomac.6b00189. PubMed PMID: 27049111.

8. Tsubota T, Yamamoto K, Mita K, Sezutsu H. Gene expression analysis in the larval silk gland of the eri silkworm Samia ricini. Insect Sci. 2016;23(6):791-804. Epub 20151022. doi: 10.1111/1744-7917.12251. PubMed PMID: 26178074.

9. Dong Y, Dai F, Ren Y, Liu H, Chen L, Yang P, Liu Y, Li X, Wang W, Xiang H. Comparative transcriptome analyses on silk glands of six silkmoths imply the genetic basis of silk structure and coloration. BMC Genomics. 2015;16(1):203. Epub 20150317. doi: 10.1186/s12864-015-1420-9. PubMed PMID: 25886738; PMCID: PMC4372302.

10. Frankenfield AM, Ni J, Ahmed M, Hao L. Protein Contaminants Matter: Building Universal Protein Contaminant Libraries for DDA and DIA Proteomics. J Proteome Res. 2022;21(9):2104-13. Epub 20220706. doi: 10.1021/acs.jproteome.2c00145. PubMed PMID: 35793413; PMCID: PMC10040255.

11. Reddy N, Yang YQ. Investigation of the Structure and Properties of Silk Fibers Produced by Actias lunas. Journal of Polymers and the Environment. 2012;20(3):659-64. doi: 10.1007/s10924-012-0482-x. PubMed PMID: WOS:000308819700004.

12. Pacheco MO, Aikman EL, Bagnis HK, Gerzenshtein IK, Truong TD, Stoppel WL. Degumming Time Governs Self-Assembled Silk Fibroin Hydrogel Properties through Molecular Weight and Amino Acid Composition. Biomacromolecules. 2025;26(8):5069-85. Epub 20250725. doi: 10.1021/acs.biomac.5c00506. PubMed PMID: 40709791.

13. Bucciarelli A, Greco G, Corridori I, Pugno NM, Motta A. A Design of Experiment Rational Optimization of the Degumming Process and Its Impact on the Silk Fibroin Properties. ACS Biomater Sci Eng. 2021;7(4):1374-93. Epub 20210217. doi: 10.1021/acsbiomaterials.0c01657. PubMed PMID: 33594891.

14. Malay AD, Sato R, Yazawa K, Watanabe H, Ifuku N, Masunaga H, Hikima T, Guan J, Mandal BB, Damrongsakkul S, Numata K. Relationships between physical properties and sequence in silkworm silks. Sci Rep. 2016;6:27573. Epub 20160609. doi: 10.1038/srep27573. PubMed PMID: 27279149; PMCID: PMC4899792.

15. Aikman EL, Eccles LE, Stoppel WL. Native Silk Fibers: Protein Sequence and Structure Influences on Thermal and Mechanical Properties. Biomacromolecules. 2025;26(4):2043-59. Epub 20250307. doi: 10.1021/acs.biomac.4c01781. PubMed PMID: 40052735.